Time reversal technique for gas leakage detection

A. O. Maksimov, and Yu. A. Polovinka

Citation: The Journal of the Acoustical Society of America **137**, 2168 (2015); doi: 10.1121/1.4916693
View online: https://doi.org/10.1121/1.4916693
View Table of Contents: https://asa.scitation.org/toc/jas/137/4
Published by the Acoustical Society of America

Time reversal technique for gas leakage detection

A. O. Maksimov[a] and Yu. A. Polovinka
Pacific Oceanological Institute, Far Eastern Branch of the Russian Academy of Sciences, Vladivostok 690041, Russia

(Received 14 October 2014; revised 7 March 2015; accepted 17 March 2015)

The acoustic remote sensing of subsea gas leakage traditionally uses sonars as active acoustic sensors and hydrophones picking up the sound generated by a leak as passive sensors. When gas leaks occur underwater, bubbles are produced and emit sound at frequencies intimately related to their sizes. The experimental implementation of an acoustic time-reversal mirror (TRM) is now well established in underwater acoustics. In the basic TRM experiment, a probe source emits a pulse that is received on an array of sensors, time reversed, and re-emitted. After time reversal, the resulting field focuses back at the probe position. In this study, a method for enhancing operation of the passive receiving system has been proposed by using it in the regime of TRM. Two factors, the local character of the acoustic emission signal caused by the leakage and a resonant nature of the bubble radiation at their birth, make particularly effective scattering with the conjugate wave (CW). Analytical calculations are performed for the scattering of CW wave on a single bubble when CW is formed by bubble birthing wail received on an array, time reversed, and re-emitted. The quality of leakage detection depends on the spatio-temporal distribution of ambient noise.
 [http://dx.doi.org/10.1121/1.4916693]

[APL] Pages: 2168–2179

I. INTRODUCTION

Leak detection is a continuously evolving area of gas and oil industry activity. Passive acoustic detection for subsea facilities uses hydrophones to detect leaks based on changes in the background noise pattern. Identifying small leaks can be a limitation to this technology as the measurement disturbed by background noise produced by vessels and agitated sea surface. Thus a sufficient drop in pressure is required for the method to be effective. Passive acoustic method has been used for bubble measurement in laboratory and geophysical systems for more than two decades.[1–12] The advantages of this method are the low power and data requirements, which give acoustics the ability to monitor continuous. It was demonstrated most notably in a recent study[12] where, by monitoring for several days continuously, the passive acoustic system revealed that the gas leaking from the seabed was greatest at low tide and least at high tide. In contrast, the divers deployed at much greater cost only managed to measure the gas flux at a single time window and could not see such a correlation with tide.

When a leak occurs, each bubble produces a particular acoustical signal, which takes the form of an exponentially decaying sinusoid. If the bubbles are generated so infrequently that the signals do not overlap, it is simple on the basis of the signal shape to estimate the number of bubbles produced and their sizes.[1,7] If the signatures partially overlap, appropriate transforms may help,[3] although if the bubble production rate is sufficiently great that individual signatures cannot be identified, a full acoustic inversion must be undertaken.[11]

Detection of acoustic signals in the ocean is always performed against a noise background. An array of sensors may provide some discrimination against noise. In time-reversal acoustics,[13–16] a signal emitted by a localized source is recorded by an array of transducers, time-reversed, and then re-transmitted into the medium. Because of the time reversibility of the wave equation, we have refocusing of the time-reversed signal at the source when there is no attenuation. Jackson and Dowling[17] developed a theoretical formalism to describe time reversal technique in the ocean. Since 1998, Kuperman *et al.*[18,19] have performed several underwater acoustics experiments in ocean waveguide to accomplish time reversal focusing. Different applications of time reversal in the ocean acoustics have been intensively studied in subsequent years.[20–26]

If the time-reversed operation is only performed on a limited angular area (a time reversal mirror, TRM), a small part of the field radiated by the source is captured and time reversed, thus limiting reversed and focusing quality. A finite angular aperture of TRM yields an increase in the point spreading function dimension[16] that is usually related to the mirror angular aperture observed from the source. One of the most promising areas for the application of TRMs is pulse-echo detection.

Temporal and spatial focusing properties of time-reversal mirrors have been studied in waveguides.[27,28] Temporal compression means that the time reversed signal at the source is similar to the signal previously emitted by the source. However, the size of the TRM is often small compared to the propagation distance, that is, the aperture of the time-reversal mirror is small, and only a small part of the

[a]Author to whom correspondence should be addressed. Electronic mail: maksimov@poi.dvo.ru

 0001-4966/2015/137(4)/2168/12/$30.00

advancing wave is captured and time reversed. In homogeneous media, the spatial resolution of the time-reversed signals is limited by diffraction and is inversely proportional to the aperture size and proportional to the wavelength times the propagation distance. If the medium is randomly inhomogeneous, the focusing resolution of the back-propagated signal can be better than the resolution in the homogeneous case.[29] The same kind of improvement may be obtained for waves propagating in a waveguide. Multiple reflections along the medium boundaries significantly increase the aperture of the TRM.[16]

For more than ten years, time-reversal techniques have been developed in different fields. In particular, this technique was used to study the bubbles. Contrast agents, usually bubbles a few microns in diameter are retained in tumor or thrombus. These micro-bubbles have a specific acoustic response allowing ultrasound imaging to distinguish them from tissue or blood. The ability of time reversal processing to focus waves through inhomogeneities on such targeted microbubbles have been studied in Ref. 30. This method was shown to efficiently correct aberration induced by heterogeneities encountered by the wave on its travel path. The same technique have been used to focus waves on cavitation bubbles induced within tissue.[31,32] Using the ability of time reversal to refocus an amplified ultrasound waves toward its initial source, a method has been derived to restrict energy deposition on localized or extended areas of tissue.

Another application of the time-reversal focusing technique was to upscale single bubble sonoluminescence from a bubble trapped in liquid by a low frequency sound field.[33] This technique leads to transmission of a much higher incident wave on the bubble. The principle is to apply pressure pulse adaptively focusing on the bubble at the time of collapse.

Analysis of time reversal for a single spherical scatterer[34] and isolating scattering resonances of an air-filled spherical shell using iterative, single-channel time reversal[35] are the studies intimately connected with the current approach proposing use of TRM for leak detection.

Phase conjugation of the acoustic waves by bubble screen and enhanced transmission of acoustic waves with bubble meta-materials have been the subject of a number of studies.[36–41] Soundproofing is a challenging task at low frequencies because it involves blocking large-wavelength waves and requires thick materials. Among possible acoustic sub-wavelength resonators bubbles seem to be interesting candidates. The ability of an ultrasound time-reversal mirror to focus inside such a bubbly metamaterial with a subwavelength resolution has been investigated in Ref. 40.

The necessity of monitoring for leak detection in subsesa carbon capture and storage facilities, methane seeps, and gas pipelines is part of what is driving this research and development of subsea detection methods. The monitoring of carbon sequestration sites and gas pipelines requires a system that is deployable for extended periods and capable of real-time bubble generation detection. One of the major limitations of existing passive methods is the uncertainty in the strength of the signals emitted by the bubbles to ensure quick and reliable subsea leak detection. The proposed technique based on the use of time-reversal signals largely eliminates this drawback because the decision of a leak detection is taken not on the basis of the original (weak) signal but from the analysis of a much more intense signal of back-scattered reversed wave.

The paper is structured as follows: In Sec. I, we describe the basic results obtained in understanding and development of the time-reversal technique. In Sec. II, we represent the theoretical model for the bubble volume oscillations and emission near a seabed. In Sec. III, TRM system with its analog in waveguide studied for leak detection. We deduce from this representation a simple way to compute, directly in the time domain, the acoustic focusing after time reversal. In Sec. IV, we study the backscattering of the time reversal wave by a bubble. Finally, we discuss the factors that influence the effectiveness of the proposed technique.

II. SOUNDS OF SUBSEA LEAKAGE

When a leak occurs, each bubble produces a particular acoustical signature, which generally varies inversely with bubble radius and takes the form of an exponentially decaying sinusoid. During the emission time $t_{em} = 2QT_0$ (about 30 cycles), where $Q \approx 15$ is the quality factor and $T_0 = R_0/327$ (T_0 is the period of natural oscillations in seconds, R_0 is the bubble equilibrium radius in centimeters), the bubble rises up at a relatively short distance $h = R_0 + ut_{em} = R_0(1 + u \times 25/327)$, where the rising velocity of millimeter sized bubbles u equals 14–25 cm/s (Ref. 42). This implies that the bubble will rise during radiation time at distances that are compared with its radius. Thus the radiation comes from a region immediately adjacent to the bottom. We consider only the simplest mechanism of injection when in single-event detachments, the appearance of a single bubble has no effect on the release of another. With a significant gas flow, the multiple excitations of the bubble can occur,[43,44] so that the dependence on quality factory Q no longer is the dominant feature.

The theoretical model for the bubble volume oscillations near the seabed has been proposed and an analytical solution has been recently derived.[45] It was shown that the bispherical coordinates provide separation of variables and are more suitable for analysis of the volume oscillations of these constrained bubbles. Explicit formulas have been derived that describe the dependence of the bubble emission near a rigid wall on its size and the separation distance between the bubble and the boundary.

In the case considered here, of natural oscillations, the solution describing variation of the pressure $P - P_\infty$ (P_∞ is the equilibrium pressure that would occur in the liquid far from the bubble if the bubble was not present) cannot contain incoming waves and has the form[45]

$$P(\boldsymbol{r}, t) - P_\infty = \frac{\rho_w}{2\pi r} \frac{\partial^2 \Delta V(t - r/c)}{\partial t^2}, \tag{1}$$

where ρ_w is the density of water and ΔV is the variation of the bubble volume during oscillations. This expression differs by a factor of 2 from the general expression for the

pressure generated by the pulsating volume in the far field. This factor reflects the fact that the presence of a rigid boundary is similar to the mirror bubble oscillating synchronously.

The variation of the bubble volume satisfies an analog of the Rayleigh equation

$$\Delta\ddot{V} + 2\beta_{tot}\frac{\partial \Delta V}{\partial t} + \Omega_*^2 \Delta V = 0,$$
$$\Omega_* = \tilde{\Omega}\Omega_0, \quad \Omega_0^2 = \frac{3\gamma P_0(1+H/10)}{\rho_w R_0^2}, \quad \kappa = \frac{h_b}{R_0},$$
$$\tilde{\Omega}^2 = 1 - 2\sqrt{\kappa^2-1}\sum_{n=0}^{\infty}\frac{\left[\kappa+\sqrt{\kappa^2-1}\right]^{-(2n+1)}}{\left[\kappa+\sqrt{\kappa^2-1}\right]^{(2n+1)}+1}. \quad (2)$$

Here Ω_* and Ω_0 are the natural frequencies of the bubble located at the distance h_b above the rigid bottom and a free bubble, respectively; γ is the polytropic exponent, P_0 is the equilibrium pressure for gas in the bubble (hydrostatic pressure is increased to one atmosphere when submerged for every 10 m), H is the depth of the water area. It should be noted that the presence of a rigid boundary decreases the natural frequency. The cofactor $\tilde{\Omega}$ describes how the distance to the boundary h_b affects the parameters of the bubble oscillations.

It has been shown[45] that the traditional method taking into account only the monopole component in the interaction between the bubble and its mirror image has a limited range of applicability and cannot be applied at distances compared with the size of the bubble. It should be emphasized that this applies for the case when the seabed is modeled as a rigid reflector. Bubble dynamics near a fluid-fluid interface (Pekeris waveguide) or an impedance wall can be described using bispherical coordinates. However, generalization of the results presented in Ref. 45 is accompanied by rather cumbersome calculations. For this reason, these results were not included in this work.

Bubble damping is described through use of a damping coefficient β_{tot}. This parameter equals the sum of three damping coefficients corresponding to viscous losses, β_v, thermal losses, β_{th}, and the acoustic radiation from the bubble itself, β_r,

$$\beta_{tot} = \beta_{th} + \beta_v + \beta_r,$$
$$\beta_v = \frac{2\nu}{R_0^2}\frac{R_0}{|\delta|\tilde{\Omega}^2}F_v(\kappa), \quad \beta_r = \frac{R_0\tilde{\Omega}^2\Omega_*^2}{c}. \quad (3)$$

Because of the high thermal conductivity and specific heat of the liquid, the thermal dissipation β_{th} of a free bubble is governed mainly by hysteresis effect in compression the gas. The rigid boundary has no appreciable effect on this mechanism of loss. We have identified three factors in the expression for the viscous damping. The first one, $2\nu/R_0^2$, characterizes the viscous losses at the free surface the bubble wall. The second factor shows how the viscous losses near the rigid wall exceed the losses at the free surface, $R_0/|\delta| \gg 1$. Note that for the millimeter sized bubbles and kilohertz frequency range, the viscous length $|\delta|$ is small compared with the equilibrium radius, R_0. The third factor, $F_v(\kappa)$, describes the law of diminishing losses with increasing distance from the bubble to the rigid wall, $\kappa = h_b/R_0$. The behavior of F_v for large values of the argument κ is given by the formula $F_v \approx 1/(4\kappa^2)$. The asymptotic approximates the behavior of F_v very well for practically all relevant values of the argument.[45] The damping constant, β_r, differs from that for a free bubble (Ref. 2) by a co-factor (Ref. 45) $2\tilde{\Omega}^2$.

Bubble detachment from a nozzle and concurrent acoustic emission have been examined by Deane and Czerski.[46] The pressure pulse radiated by the bubble shows that the acoustic excitation begins just before detachment and is largely complete within a single oscillation. Authors came to conclusions that the sound produced by a bubble can be explained by the collapse of the neck of air formed immediately after bubble pinch-off. A good approximation to describe the shape of the emitted acoustic pulse $p(\boldsymbol{r},t) = P(\boldsymbol{r},t) - P_\infty$ is the following expression:

$$p(\boldsymbol{r},t) = -\frac{p_0}{2\pi}\left(\frac{R_0}{r}\right)\exp[-\beta_{tot}(t-t_0-r/c)] \times \sin[\Omega_*(t-t_0-r/c)]\Theta(t-t_0-r/c). \quad (4)$$

Here p_0 is the pulse amplitude and t_0 is the time of pinch-off. More complex behavior at the beginning of the first half-period leads to the generation of high-frequency components, which are likely to be heavily damped, when they propagate in the range of tens to hundreds of meters to an array of source/receiver transducers (SRT). Equation (4) is valid at distances smaller than the characteristic scale of variation of the sound speed and accounts for the presence of the rigid wall (seabed) which modifies free bubble oscillations.

The results presented in this section are based on certain key simplifications. Specifically, it is assumed that the seabed behaves as a rigid acoustic boundary and that the bubble injection occurs as if the bubbles are slowly released one by one from the seabed. In simple single-event detachments, the appearance of a single bubble has no effect on the release of another. These might not be true in real leaks, and we consider the proposed model as a first order approximation to the real scenario. It should be noted that these results are valid for single isolated bubble injections, and the conclusions cannot automatically be extrapolated to the cases of Ref. 43, which would be more reminiscent of a gas leak form a facility or pipe.

III. TIME-REVERSAL OF BUBBLE EMISSION

A time-reversal process exploits the time-reversal invariance of the wave equation such that the transmitted wave from a TRM converges back to the position of a source (see Fig. 1). The fact that time-reversal processing both spatially and temporally refocuses the acoustic energy in a complicated ocean environment suggests possible application for detecting and localization of weak acoustic signals emitted at underwater leakage.

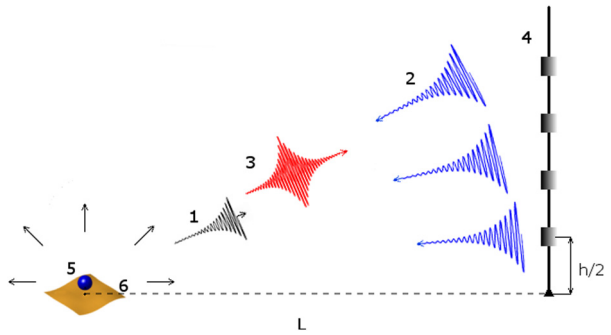

FIG. 1. (Color online) Illustration of the set-up for array time reversal of the bubble birthing wail from the sandy seabed. Numbers in the figure denote the following elements: (1) The pressure pulse radiated by the bubble at its birth, (2) the time reversed signals emitted by the elements of source/receiving array, (3) the back-scattering signal generated by resonant interaction between the time-reversed wave and a bubble, (4) the source/receiving array, (5) a gas bubble birthing at the leakage, and (6) seabed. The horizontal distance between the bubble and the vertical array is L and the separation between the transducers in the array is $h/2$.

The basic time-reversal experiment[14] can be described in the following way: As a first step, a point-like source located at $\mathbf{r}_0$ emits a pulse at $t = t_0 \geq 0$ (for the convenience of calculations, we take $t_0 = 0$). In our case, a small active source (bubble) is located at $\mathbf{r}_0 = (0,0,0)$ and the shape of the signal is described by expression (4). The array has point transducers located at $\mathbf{r}_j = (0, L, jh/2)$, for $j = 1, 2, \ldots, N$. The separation $h/2$ between array elements is chosen so that the transducers behave like an array of aperture $a = N \cdot h/2 \ll L$. Often $h = \lambda_0$, the wavelength of the carrier frequency of the pulse.

In a medium without attenuation, we choose the scalar wave equation as our mathematical model for wave propagation. At frequency ω, the two point, outgoing Green's function between points A (in $\mathbf{r}_0$) and B (in $\mathbf{r}$) satisfies the Helmholtz equation, which in cylindrical coordinates with the range coordinate $\boldsymbol{\rho} = (x, y)$ and the depth coordinate denoted by z has the form

$$\nabla^2 G_\omega(\boldsymbol{\rho} - \boldsymbol{\rho}_0; z, z_0) + k^2(z) G_\omega(\boldsymbol{\rho} - \boldsymbol{\rho}_0; z, z_0) = -\delta(\boldsymbol{\rho} - \boldsymbol{\rho}_0)\delta(z - z_0), \tag{5}$$

where $k^2(z) = \omega^2/c^2(z)$ and c is the sound speed in the medium. Letting ρ be the horizontal distance from the source, Eq. (5) has the far field, azimuthal symmetric normal mode solution for the pressure given by[21]

$$G_\omega(\rho; z, z_0) = \mathrm{i}[\rho_w(z_0)(8\pi\rho)^{1/2}]^{-1} \exp(-\mathrm{i}\pi/4) \times \sum_n k_n^{-1/2} u_n(z) u_n(z_0) \exp(\mathrm{i}k_n\rho). \tag{6}$$

Here $\rho_w^{-1}(z_0)$ is the weighting function, the local density, u_n, k_n are the normal mode Eigenfunctions and modal wave numbers obtained by solving the following eigenvalue problem:

$$\frac{d^2 u_n}{dz^2} + [k^2(z) - k_n^2] u_n(z) = 0. \tag{7}$$

A good approximation is to use a set of discrete mode functions obtained from a waveguide extended in depth and terminated by a pressure release and rigid boundaries.[21]

Application of an approximation in which we ignore the layered structure of the ocean, leads to the following form of the Green's function:

$$G_\omega(\boldsymbol{\rho} - \boldsymbol{\rho}_0; z, z_0) = \frac{1}{4\pi}\left(\frac{e^{\mathrm{i}kR_{01}}}{R_{01}} + \frac{e^{\mathrm{i}kR_{02}}}{R_{02}}\right);$$
$$R_{0m} = \sqrt{(\boldsymbol{\rho} - \boldsymbol{\rho}_0)^2 + z_{0m}^2}; \quad m = 0, 1;$$
$$z_{01} = z - z_0, \quad z_{02} = z + z_0, \tag{8}$$

which accounts for a presence of the rigid boundary (seabed) at $z = 0$. Classically the Green's function is written as a diverging spherical wave (homogeneous and free space case) and additional terms that describe the interaction of the field with the boundaries.

The Fourier transform of the source pulse is determined from Eq. (4),

$$S(\omega) = \frac{p_0 R_0 \Omega_*}{\omega^2 - \Omega_*^2 - \beta_{tot}^2 + 2\mathrm{i}\omega\beta_{tot}}. \tag{9}$$

The jth element of the SRA receives the following time-domain signal:

$$p(\rho, z_j; t) = \int G_\omega(\rho; z_j, z_0) S(\omega) e^{-\mathrm{i}\omega t} d\omega. \tag{10}$$

For the limiting case when the frequency-domain Green's function has the form [Eq. (8)], the received pressure field is transformed to

$$p(\rho, z_j; t) = \frac{p_0}{2\pi R_{01}(j)} e^{-\mathrm{i}\Omega_*\left(t - R_{01}(j)/c\right)} \times e^{-\beta_{tot}\left(t - R_{01}(j)/c\right)} e^{\mathrm{i}\pi/2} \Theta\left(t - R_{01}(j)/c\right). \tag{11}$$

We assume that we are able to measure the pressure field at any element of array during the interval $[0, T]$. As time-reversal experiments are based on a two-step process, the measurement step must be limited in time by a parameter T. During the second step of the time-reversal process, we create on the elements of the array the signal that corresponds to the time reversal of those same components measured during the first step. The time-reversal operation is described by the transform $t \to T - t$. The received signal has the form of a decaying exponent and is significantly different from zero only during the characteristic decay time $\tau \approx \beta_{tot}^{-1}$. Then the time-reversal signal that will be used to excite the jth transmitting element of the array is $p(\rho, z_j; T - t)$ such that $T > 2\tau$. This condition is imposed by causality: The signal has to be completely received before it can be time reversed.

The explicit form of the reversed signal is given by the following integral,[21]

$$p(\rho, z_j; T - t') = \int G_\omega(\rho; z_j, z_0) S(\omega) e^{-\mathrm{i}\omega(T - t')} d\omega = \int [G_\omega^*(\rho; z_j, z_0) S^*(\omega) e^{\mathrm{i}\omega T}] e^{-\mathrm{i}\omega t'} d\omega, \tag{12}$$

where t' is the radiation time measured from the moment T and the conjugate symmetry of the frequency-domain Green's function and probe pulse has been used.

The bracketed quantity in Eq. (12) is the frequency-domain representation of the signal retransmitted by the jth element of the array. Fourier synthesis can be used to obtain the time-domain representation of the field produced by time-reversal mirror[21]

$$p^{tr}(\rho_{tr}, z_1; t_1) = \sum_{j=1}^{N} \int G_\omega(\rho_{tr}; z_1, z_j)\, G^*_\omega(\rho; z_j, z_0) \times e^{i\omega T} g S^*(\omega) e^{-i\omega t_1} d\omega. \quad (13)$$

Here t_1 specifies the moment of observation of the reversal field at the point $\mathbf{r}_1 = (\boldsymbol{\rho}_1, z_1)$ (measured from the moment T), $\rho_{tr} = \sqrt{x_1^2 + (y_1 - L)^2}$ is the horizontal distance from the array $\boldsymbol{\rho} = (0, L)$ to the observation point $\boldsymbol{\rho}_1 = (x_1, y_1)$, g and R_t are the amplification coefficient and the scale of the emitted signal ($R_t \approx 1$ m). The signal received by the array after amplification, time reversal, and time delay is emitted and propagates in the medium. This expression incorporate all waveguide effects, including time elongation due to multipath propagation.

For the limiting case of free half-space bounded by the rigid boundary, an analytical solution for the problem can be obtained

$$p^{tr}(\rho_{tr}, z_1; t_1) = \sum_{j=1}^{N} \int \frac{p_0 g R_0 R_t \Omega_* e^{-i\omega(t_1 - T)} d\omega}{\omega^2 - \Omega_*^2 - \beta_{tot}^2 - 2i\omega\beta_{tot}} \times \left[\frac{e^{ikR^{tr}_{01}(j)}}{R^{tr}_{01}(j)} + \frac{e^{ikR^{tr}_{02}(j)}}{R^{tr}_{02}(j)} \right] \frac{e^{-ikR_{01}(j)}}{16\pi^2 R_{01}(j)}. \quad (14)$$

To evaluate Eq. (14), the integrand is extended to the complex plane, and the contour integral is then determined by calculating the sum of the residues of its poles $\omega = \pm\Omega_* + i\beta_{tot}$,

$$p^{tr}(\rho_{tr}, z_1; t_1) = -\frac{g p_0}{8\pi} \sum_{j=1}^{N} \frac{R_0}{R_{01}(j)} \left\{ \left[R_t / R^{tr}_{01}(j)\right] \sin\left(\Omega_* \tau^{(1)}_+\right) e^{-\tau^{(1)}_+ \beta_{tot}} \Theta\left(\tau^{(1)}_+\right) \Theta\left(\tau^{(2)}_+\right) + \left[R_t / R^{tr}_{02}(j)\right] \sin\left(\Omega_* \tau^{(1)}_-\right) e^{-\tau^{(1)}_- \beta_{tot}} \Theta\left(\tau^{(1)}_-\right) \Theta\left(\tau^{(2)}_-\right) \right\},$$
$$\tau^{(1)}_{+,-} = T - t_1 + (R^{tr}_{01,2}(j) - R_{01,2}(j))/c, \quad \tau^{(2)}_{+,-} = t_1 - R^{tr}_{01,2}(j)/c. \quad (15)$$

The positions of the leading and trailing edges of the direct pulse are determined by the conditions $\tau^{(1)}_+ = 0$ and $\tau^{(2)}_+ = 0$, respectively. For the pulse reflected by the rigid boundary that corresponds to propagation from the mirror source ($x = 0$, $y = L$, $z = -z_j$), these conditions take the form $\tau^{(1)}_- = 0$ and $\tau^{(2)}_- = 0$.

We consider the back propagating field at a "search" point $\mathbf{r}_1 = (\boldsymbol{\rho}_1, z_1)$ located in the plane determined by the bubble and the array. The linear vertical array can provide focusing only in this plane. In a remote sensing regime ($a \ll L$, $a = hN/2$), we can use the parabolic approximation of the phase[47]

$$R^{tr}_{01,2}(j) = \sqrt{(L - \Delta y)^2 + (\Delta z \mp z_j)^2} \approx L - \Delta y + (\Delta z \mp z_j)^2 / 2L,$$
$$R_{01}(j) = \sqrt{L^2 + z_j^2} \approx L + z_j^2 / 2L. \quad (16)$$

Then using this approximation in Eq. (15) at $\mathbf{r}_1 = (0, \Delta y, \Delta z)$, we have

$$p^{tr}(0, \Delta y, \Delta z; t_1) = -\frac{g p_0 R_0 R_t}{8\pi L^2} \sum_{j=1}^{N} \left\{ \sin\left(\Omega_* \tau^{(1)}_+\right) e^{-\tau^{(1)}_+ \beta_{tot}} \Theta\left(\tau^{(1)}_+\right) \Theta\left(\tau^{(2)}_+\right) + \sin\left(\Omega_* \tau^{(1)}_-\right) e^{-\tau^{(1)}_- \beta_{tot}} \Theta\left(\tau^{(1)}_-\right) \Theta\left(\tau^{(2)}_+\right) \right\},$$
$$\tau^{(1)}_{\pm} = T - t_1 - \Delta y/c + \left(\Delta z^2 \mp 2\Delta z z_j\right)/(2Lc), \quad \tau^{(2)}_{\pm} = t_1 - (L - \Delta y)/c - \left(\Delta z \mp z_j\right)^2/(2Lc). \quad (17)$$

Note that $R^{tr}_{01,2}$ and R_{01} are approximated by L in the amplitude. Because $z_j = hj/2$ are small (with respect to a and L), we approximate the sum in Eq. (17) by an integral. In leading order, the dependence on the variable of integration is presented only in the exponent: $\exp[-i(\Omega_* + i\beta_{tot})(\Delta z w / Lc)$. The limits of integration depend on time at passing of the leading and trailing edges of the pulse through the point of observation. The positions of edges are determined by Θ functions.

The position of the leading edge of the pulse 'illuminated' by the wth element of the aperture is given by $t_{ld} = (L - \Delta y)/c + (\Delta z - w)^2/(2Lc)$. The signal appears at the observation point at time $t_a = (L - \Delta y)/c$, $w_* = \Delta z$ and its

amplitude increases from 0. The transition process lasts as long as the all elements of the array will illuminate the observation point. During the time interval $t_{ld} > t_a$, the limits of integration for w are determined from the condition $w_{\pm} = \Delta z \pm \sqrt{2Lc(t_1 - t_a)}$. At time $t_{ld+} = t_a + (a - \Delta z)^2/(2Lc)$, $w_+ = a$, the upper limit of integration reaches the boundary of the aperture, and it will be constant during the next time interval. At time $t_{ld-} = t_a + (a + \Delta z)^2/(2Lc)$, $w_- = -a$, the illumination of the observation point will be implemented by the entire aperture of the array:

$$p^{tr}(0,\Delta y,\Delta z;t_1) = -\frac{gp_0R_0R_t}{4\pi hL^2}\frac{1}{2\mathrm{i}}\left\{f(\Delta y,\Delta z;t_1)\exp\{\mathrm{i}(\Omega_* + \mathrm{i}\beta_{tot})[T - t_1 - \Delta y/c + \Delta z^2/(2Lc)]\} - c.c.\right\}$$
$$f(\Delta y,\Delta z;t_1) = \int_{-a}^{a} dw e^{-\mathrm{i}(\Omega_* + \mathrm{i}\beta_{tot})(\Delta z w/Lc)}\Theta\left(T - t_1 - \Delta y/c + (\Delta z^2 - 2\Delta z w)/(2Lc)\right)$$
$$\times\,\Theta\left(t_1 - (L - \Delta y)/c - (\Delta z - w)^2/(2Lc)\right). \tag{18}$$

The position of the trailing edge of the pulse is given by $t_{tl} = T - \Delta y/c + \Delta z^2/(2Lc) - (\Delta z w)/(Lc)$. At time $t_{tl+} = T - \Delta y/c + \Delta z^2/(2Lc) - \Delta z a/(Lc)$, the upper element of the aperture stops emitting. The entire array stops emitting at time $t_{tl-} = T - \Delta y/c + \Delta z^2/(2Lc) + \Delta z a/(Lc)$. Pulse duration $t_{tl-} - t_a = T - L/c + \Delta z^2/(2Lc) + a\Delta z/(Lc)$ increases with the distance from the source Δz (the point at which reversal signal is focusing).

Thus the pulse shape has the following form

$$p^{tr}(0,\Delta y,\Delta z;t_1) = \frac{gp_0R_0R_t}{4\pi hL}P_N(0,\Delta y,\Delta z;t_1);$$
$$P_N(0,\Delta y,\Delta z;t_1) = -\frac{c}{\Delta z\sqrt{\Omega_*^2 + \beta_{tot}^2}}$$
$$\times\begin{cases}
0, & t_1 < t_a,\\
\left\{\cos\left[\Omega_*\left(t_{tl+} - t_1 + \frac{\Delta z}{Lc}\left(a - \Delta z - \sqrt{2Lc(t_1 - t_a)}\right)\right) + \varphi\right]\right. & \\
\quad\times\exp\left\{-\beta_{tot}\left[t_{tl+} - t_1 + \frac{\Delta z}{Lc}\left(a - \Delta z - \sqrt{2Lc(t_1 - t_a)}\right)\right]\right\} & \\
\quad -\cos\left[\Omega_*\left(t_{tl-} - t_1 - \frac{\Delta z}{Lc}\left(a + \Delta z - \sqrt{2Lc(t_1 - t_a)}\right)\right) + \varphi\right] & \\
\left.\quad\times\exp\left\{-\beta_{tot}\left[t_{tl-} - t_1 - \frac{\Delta z}{Lc}\left(a + \Delta z - \sqrt{2Lc(t_1 - t_a)}\right)\right]\right\}\right\}, & t_a \le t_1 \le t_{ld+},\\
\left\{\cos\left[\Omega_*(t_{tl+} - t_1) + \varphi\right]e^{-\beta_{tot}(t_{tl+} - t_1)} - \cos\left[\Omega_*\left(t_{tl-} - t_1 - \frac{\Delta z}{Lc}\left(a + \Delta z - \sqrt{2Lc(t_1 - t_a)}\right)\right) + \varphi\right]\right. & \\
\left.\quad\times\exp\left\{-\beta_{tot}\left[t_{tl-} - t_1 - \frac{\Delta z}{Lc}\left(a + \Delta z - \sqrt{2Lc(t_1 - t_a)}\right)\right]\right\}\right\}, & t_{ld+} \le t_1 \le t_{ld-},\\
\left\{\cos\left[\Omega_*(t_{tl+} - t_1) + \varphi\right]e^{-\beta_{tot}(t_{tl+} - t_1)} - \cos\left[\Omega_*(t_{tl-} - t_1) + \varphi\right]e^{-\beta_{tot}(t_{tl-} - t_1)}\right\}, & t_{ld-} \le t_1 \le t_{tl+},\\
\left\{\cos\varphi - \cos\left[\Omega_*(t_{tl-} - t_1) + \varphi\right]e^{-\beta_{tot}(t_{tl-} - t_1)}\right\}, & t_{tl+} \le t_1 \le t_{tl-},\\
0, & t_{tl-} < t_1,
\end{cases} \tag{19}$$

where the following notation has been introduced $\varphi = -\arctan\beta/\Omega_* \ll 1$.

Figure 2(a) illustrates the shape of the time-reversal signal P_N given by Eq. (19) for the characteristic values of parameters: $\Omega_*/2\pi = 1200$ Hz, $Q = 15$, $T = 100$ ms, $a = 20$ m, $L = 100$ m, $\Delta z = 1$ m, $\Delta y = 0$, c = 1500 m/s. Under these conditions, the determining time scales take the following values: $2\pi/\Omega_* = 0.8$ ms, $\beta_{tot}^{-1} = 4$ ms, $t_a = 66.7$ ms,

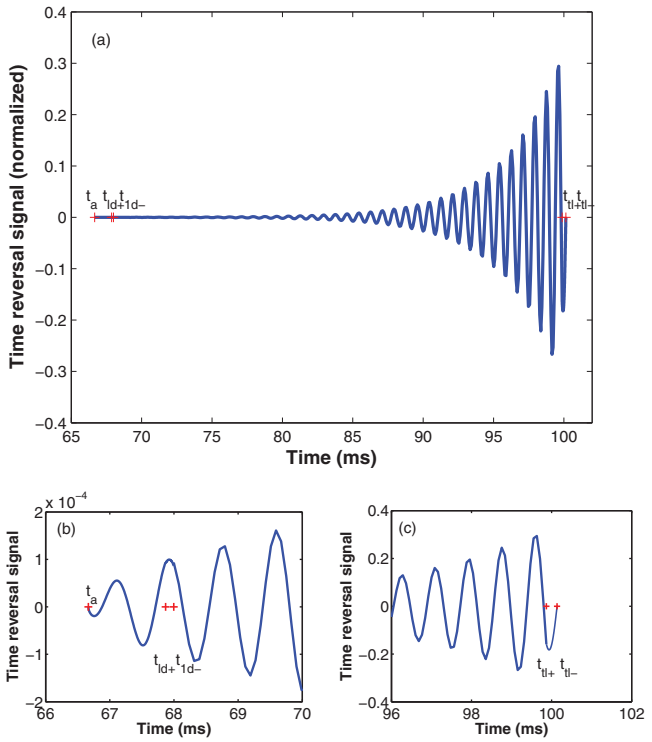

FIG. 2. (Color online) Normalized time reversal signal P_N at the observation point (0,0,1) (m) according to Eq. (19) (a). The details of the leading and trailing edge distortions are presented in (b) and (c). The characteristic time scales t_a, t_{ld+}, t_{ld-}, and t_{tl+}, t_{tl-} are shown with a plus sign. The pulse arrives at the observation point at $t_a = L/c = 66.7$ ms. Calculations have been performed for the following values of determining parameters: The period of bubble natural oscillations is $2\pi/\Omega_* = 1200$ Hz, the quality factor is $Q = 15$, the time window is $T = 100$ ms, the aperture is $a = 20$ m, the horizontal distance from the array to the observation point is $L = 100$ m.

$t_{ld+} = 67.9$ ms, $t_{ld-} = 68.2$ ms, $t_{tl+} = 99.9$ ms, $t_{tl-} = 100.1$ ms. Figures 2(b) and 2(c) illustrate the deformation of the leading and tailing edges. For a typical situation, these deformations occur in a time interval not exceeding the period of oscillations and, therefore, have little significance. However, when the source is located at large distances from the array $L \approx cT$ and

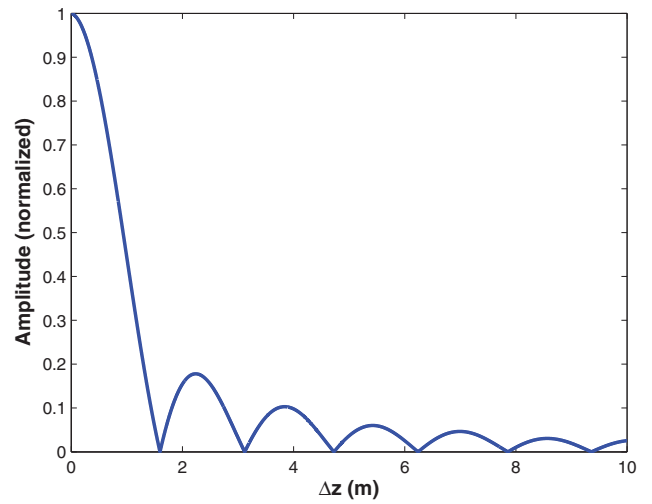

FIG. 3. (Color online) Spatial diffraction pattern of the amplitude p_n of Eq. (19) at time $t_1 = t_{tl+} - \pi/(4\Omega_*)$ normalized (relative to their maximum value). Calculations were performed for the same values of the input parameters that were used with the drawing of a graph in Fig. 2.

when it is necessary to evaluate the scattering of the reversal wave by the bubbles risen up to a distance $\Delta z \approx a$ above the source, one needs to take into account these distortions.

To estimate the spatial focusing resolution, let us consider normalized pressure amplitude $p_n = |p^{tr}(0, \Delta y, \Delta z; t_1)/p^{tr}(0,0,0;t_1)|$ above the source $\Delta y = 0$, at time $t_1 = t_{tl+} - \pi/(4\Omega_*)$. A plot of p_n is shown in Fig. 3. In the considered case of a narrow-band pulse $\Omega_* \gg \beta_{tot}$, the resolution limit comes from oscillating trigonometric functions. The dominant term is $\Omega_* a \Delta z/Lc$, and we have $\Delta z_{res} \approx L\lambda_*/a$ ($\lambda_* = 2\pi c/\Omega_*$). In either case, the larger the aperture a, the better the focusing.

The results presented in the preceding text describe a diffractive structure of the reversed field near the focal point with the characteristic spatial scale of 1 m. In reality, it is sufficient to consider a much shorter distances from the source to describe the impact of the time-reversed wave on the bubble emitted source signal. This bubble will rise at a very small distance (the rising velocity of millimeter sized bubbles equals 14–25 cm/s) during the time of propagation of the signal to the array and back.

In this case ($\mathbf{r}_1 = 0$), the behavior of the field can be found directly without resorting to approximations.

$$p^{tr}(0,0,0;t_1) = -\frac{g p_0 R_0 R_t}{4\pi h} \sin\Omega_*(T-t_1) e^{-\beta_{tot}(T-t_1)} \times \Theta(T-t_1) \int_{-a}^{a} \frac{dw}{L^2+w^2} \times \Theta\left(t_1 - \sqrt{(L^2+w^2)}/c\right). \quad (20)$$

A direct calculation of the integral in Eq. (20) gives

$$p^{tr}(0,0,0;t_1) = -\frac{g p_0 R_0 R_t}{2\pi h L} \sin\Omega_*(T-t_1) e^{-\beta_{tot}(T-t_1)} \times \begin{cases} 0, & t_1 < t_{a0}, \\ \arctan\sqrt{(t_1 c/L)^2 - 1}, & t_{a0} \le t_1 \le t_{ld0}, \\ \arctan a/L, & t_{ld0} \le t_1 \le T, \\ 0, & T < t_1, \end{cases} \quad (21)$$

where $t_{a0} = L/c$, $t_{ld0} = \sqrt{L^2+a^2}/c$. Note that the solution [Eq. (21)] expanded until the first order in the parameter a/L coincides with the approximate solution [Eq. (19)] considered in the limit $\Delta y \to 0$, $\Delta z \to 0$. Because $t_{ld0} - t_a$ is of the second order magnitude in a/L, there are no distortions of the pulse edges in this approximation.

As an illustration of the normal mode representation of the time-reversal field,[27,28] we consider an isovelocity waveguide of depth H bounded above by a pressure-release surface and below by a rigid bottom. In the experimental configuration, λ_* is always much smaller than the characteristic lengths of the waveguide L and H. In this case, the two point, outgoing Green's function [Eq. (6)] has the following form[48]

$$G_\omega(\rho; z, z_0) = \sum_{l=0}^{\infty} \frac{(-1)^l}{4\pi} \left[\frac{e^{ikR_{l1}}}{R_{l1}} - \frac{e^{ikR_{l2}}}{R_{l2}} + \frac{e^{ikR_{l3}}}{R_{l3}} - \frac{e^{ikR_{l4}}}{R_{l4}}\right], \quad (22)$$

where

$$R_{lm} = (\rho^2 + z_{lm}^2)^{1/2}; \quad l = 0, 1, 2, \ldots; \quad m = 1, 2, 3, 4;$$
$$z_{l1} = 2Hl + z - z_0; \quad z_{l2} = 2H(l+1) - z - z_0;$$
$$z_{l3} = 2Hl + z + z_0; \quad z_{l4} = 2H(l+1) - z + z_0. \tag{23}$$

The bubble will then appear to be emitted from a set of virtual sources in free space. These sources are the images of the actual source with respect to the waveguide interfaces. Because the bubble is located at a short distance from the bottom (two orders of magnitude smaller than the wavelength), z_0 can be equal to zero in the Eq. (23), and there will be only doubled terms with $m = 1$ and $m = 2$ in Eq. (23).

At radiation of a pulse signal by a single bubble [see Eq. (1)], the total field in the waveguide at the point ρ, z at time t is equal to

$$p(\rho; z, z_0; t) = \sum_{l=0}^{\infty} \frac{(-1)^l \rho_w}{2\pi} \times \left[\frac{\Delta\ddot{V}(t - R_{l1}/c)}{R_{l1}} - \frac{\Delta\ddot{V}(t - R_{l2}/c)}{R_{l2}} \right]. \tag{24}$$

The transmitted field recorded on the jth element of the array after propagation through the waveguide has the form of Eq. (24) with $z = z_j$. After arrival of a first wavefront corresponding to the direct path, there will be the arrival of a set of multipath signals corresponding to the multiple reflections of the incident wave on the interfaces. If the duration of the emitted pulse is β_{tot}^{-1}, then the receiving point at time t will fall not all impulses, but only those for which the condition $0 \le t - R_{lm} \le \beta_{tot}^{-1}$ is fulfilled. For small depths, $(R_{l+1,m} - R_{lm})/c < \beta_{tot}^{-1}$ arrived pulses overlap.

Using an analogy with the considered case of direct propagation, we obtain an explicit expression for the field of the reversed wave

$$p^{tr}(\rho_{tr}, z_1; t_1) = -\frac{g p_0 R_0 R_t}{4\pi h} \sum_{l=0}^{\infty}\sum_{n=0}^{\infty} (-1)^{l+n} \times \int_0^a dw \sum_{m=1}^{4} (-1)^{m+1} \Theta\left(t_1 - R_{nm}^{tr}/c\right) \times \left[\frac{\sin(\Omega_* \tau_{l1}^{nm}) e^{-\beta_{tot}\tau_{l1}^{nm}}}{R_{nm}^{tr} R_{l1}} \Theta\left(\tau_{l1}^{nm}(w)\right) - \frac{\sin(\Omega_* \tau_{l2}^{nm}) e^{-\beta_{tot}\tau_{l2}^{nm}}}{R_{nm}^{tr} R_{21}} \Theta\left(\tau_{l2}^{nm}(w)\right) \right], \tag{25}$$

where

$$R_{n1}^{tr} = [(\rho^{tr})^2 + (z_1 - w + 2Hn)^2]^{1/2},$$
$$R_{n2}^{tr} = [(\rho^{tr})^2 + (-z_1 - w + 2H(n+1))^2]^{1/2},$$
$$R_{n3}^{tr} = [(\rho^{tr})^2 + (z_1 + w + 2Hn)^2]^{1/2},$$
$$R_{n4}^{tr} = [(\rho^{tr})^2 + (-z_1 + w + 2H(n+1))^2]^{1/2},$$
$$\tau_{l1}^{nm}(w) = T - t_1 + R_{nm}^{tr}/c - R_{l1}/c,$$
$$\tau_{l2}^{nm}(w) = T - t_1 + R_{nm}^{tr}/c - R_{l2}/c. \tag{26}$$

Because the range of leak detection is not very large (hundreds of meters), then the antenna can get a limited number of signals propagating along different paths in the waveguide during the time corresponding to the observation window T (say five corresponding to five reflections on the interfaces). After propagation through the waveguide, the incident field depends on the interference between these five echoes. Suppose now[28] that we time-reversed the field by a TRM made of 20 transducers. We are interested in the time-reversed field in the plane of the source. Because of reciprocity, the impulse response between the TRM and the source is still made of five echoes. This means that each TRM transducer time-reverses five echoes and that each of these five echoes generates five echoes. For a 20-transducer TRM, the total number of echoes received after time reversal at each point in the plane of the source is then equal to 500.

At first glance,[28] because of the big number of echoes interfering together after time reversal, the time-reversed field appears not to be very sensitive to the phase and to the amplitude of each of them. However, the sum in Eq. (25) includes very different types of terms. The contributions of those with $R_{nm}^{tr} = R_{l1}$, $R_{nm}^{tr} = R_{l2}$ are summing coherently, and their interference is nothing more than the addition that causes the focusing effect. In contrast, the elements of the other types, add incoherently and create a diffraction pattern on which the directivity pattern of the time-reversed field is based.

By analogy with the considered above case of direct propagation Eq. (20), the contribution of coherent terms is described by the following formula:

$$p_{coh}^{tr}(0,0,0;t_1) = -\frac{g p_0 R_0 R_t}{4\pi h} \sin\Omega_*(T - t_1) e^{-\beta_{tot}(T-t_1)} \times \Theta(T - t_1) \sum_{n=0}^{R_{n1}/c + \beta_{tot}^{-1} \le T} (2 - \delta_{n,0}) \times \int_{-a}^{a} dw \frac{\Theta\left(t_1 - R_{n1}^{tr}/c\right)}{R_{n1}^2}. \tag{27}$$

A direct calculation of the integral in Eq. (27) gives

$$p_{coh}^{tr}(0,0,0;t_1) = \frac{g p_0 R_0 R_t}{4\pi h L} = P_N(t_1),$$
$$P_N(t_1) = -E(t_1)\sin\Omega_*(T - t_1) e^{-\beta_{tot}(T-t_1)},$$
$$E(t_1) = \sum_{n=0}^{R_{n1}/c + \beta_{tot}^{-1} \le T} (2 - \delta_{n,0}) \times \begin{cases} 0, & t_1 < t_{an}, \\ \arctan\dfrac{\sqrt{c^2(t_1^2 - t_{an}^2) + (2Hn + a)^2}}{L} + \arctan\dfrac{a - 2Hn}{L}, & t_{an} \le t_1 \le t_{ldn} \\ \arctan\dfrac{a + 2Hn}{L} + \arctan\dfrac{a - 2Hn}{L}, & t_{ldn} \le t_1 \le T, \\ 0, & T < t_1. \end{cases} \tag{28}$$

Here, P_N is the normalized signal, E is the envelope, $t_{an} = \sqrt{L^2 + (2Hn - a)^2}/c$ and $t_{ldn} = \sqrt{L^2 + (2Hn + a)^2}/c$ are the characteristic time scales. One should note that this expression is only part (coherently interfering at the location of the point source) of the total field. So the signals will come at the source point and after the time T, but all of them will add incoherently and lead to the formation of the noise base.

Figure 4 shows a temporal focusing of the time reversed field at the initial source.

Calculations have been performed for the same values of the input parameters that were used with the drawing of a graph in Fig. 2. Letting the waveguide depth $H = 30$ m, we focused on the parameters of the Nord Stream through the Baltic sea where an average depth runs near 55 m. Only three pulses corresponding to different paths can be caught by receiver during this window T: $n = 0, 1, 2$. The first pulse arrives at the location of the source in the moment $t_{a0} = 66.7$ ms, the second at $t_{a1} = 71.8$ ms, and the third at $t_{a2} = 94.3$ ms. These and the characteristic times t_{ld0}, t_{ld1} are shown by plus signs in Fig. 5.

Two major points are to be underlined: From the temporal point of view, multipath effects are compensated. The signal measured at the source in the waveguide is nearly identical to the one you would find after a time-reversal experiment near a rigid boundary. Second, the time-reversal focusing leads to the increasing the signal amplitude in comparison to the one observed after a time-reversal experiment with the same TRM in free half-space with a rigid boundary. In the illustrative example being discussed, this yields approximately a twofold increase in the amplitude.

IV. RESONANT SCATTERING OF THE TIME-REVERSAL WAVE BY A BUBBLE

We analyze scattering of the time reversal wave by a single bubble in the conditions when the radius of the bubble is much smaller than the acoustic wavelength λ_* (i.e., $R_0/\lambda_* = R_0\Omega_*/c \ll 1$). In this case, there is effectively an inner region around the bubble that may be regarded as incompressible. The volume oscillations of the constrained bubbles were recently analyzed,[45,49,50] and an analytical solution of this problem has been obtained by using special (toroidal and bispherical) coordinate systems. The constraint hampers acceleration of liquid at the bubble wall. This leads to an increase in the inertial mass and thus to a lowering of the natural frequency of the volume oscillations.

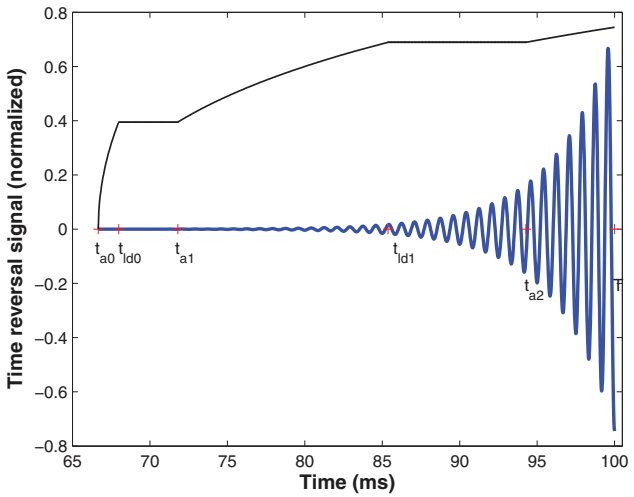

FIG. 4. (Color online) Time-reversal signal P_N (thick solid line) and its envelope E (thin line) in waveguide at the location of the source. Curves correspond to the normalized values that are described by Eq. (28) with the input data: $a = 20$ m, $c = 1500$ m/s, $L = 100$ m, $H = 30$ m, $\Omega_*/2\pi = 1200$ Hz, $Q = 15$, and the time window $T = 100$ ms. The characteristic time scales coming in Eq. (28) are shown by plus signs.

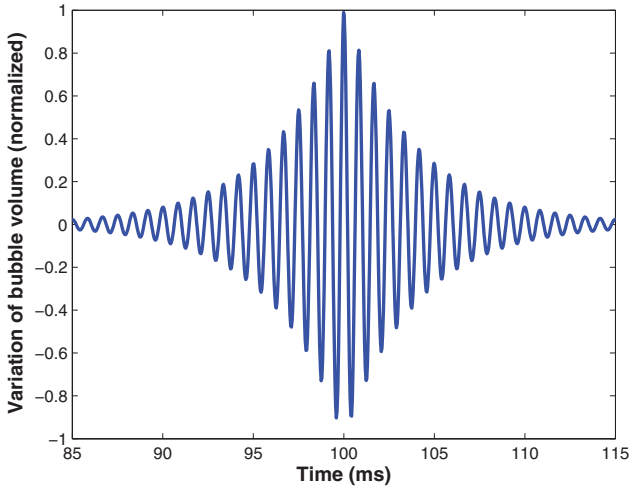

FIG. 5. (Color online) Normalized (relative to their maximum value) variations in the bubble volume driven by time-reversal signal. The time-reversed signal arrives at the place of bubble location at $L/c = 66.7$ ms, the period of bubble natural oscillations is 1200 Hz, the quality factor, Q, equals to $Q = 15$, and the time of measurement, T, is $T = 100$ ms.

An analog of Rayleigh equation for the volume pulsation of the bubble near a rigid wall under action of the time-reversal wave has the form[45]

$$\Delta\ddot{V} + 2\beta_{tot}\frac{\partial \Delta V}{\partial t} + \Omega_*^2 \Delta V = -\frac{4\pi R_0}{\rho_w \tilde{\Omega}^2} p^{tr}(0,0,0;t). \quad (29)$$

Note that in the description of the time-reversal field the presence of the rigid bottom has been taken into account: The Green's function is formed by the sum of the direct and mirror sources.

The method of Green's functions can be used to solve this equation

$$\Delta V(t) = \frac{4\pi R_0}{\rho_w \tilde{\Omega}^2 \Omega_*} \int_0^t p^{tr}(0,0,0;\tau) e^{-\beta_{tot}(t-\tau)} \times \sin\Omega_*(t-\tau)\, d\tau. \quad (30)$$

The presence of Θ functions in the explicit expression for p^{tr} [see Eq. (21)] leads to the fact that the lower limit of integration is L/c, and the upper one, depending on the ratio of t and T, is either $t(t \le T)$ or $T(t \ge T)$. The result of direct calculations leads to the following expression for the variation of the bubble volume:

$$\Delta V(t) = \frac{g p_0 R_0^2 R_t \Omega_*}{4\rho_w \tilde{\Omega}^2 hL} \arctan\left(\frac{a}{L}\right) \times \left\{ \frac{\cos\Omega_*|t-T|}{\beta_{tot}} e^{-\beta_{tot}|t-T|}\left(1 - e^{-2\beta_{tot}(t-L/c)}\right) - \frac{1}{\sqrt{\Omega_*^2 + \beta_{tot}^2}} \left[\cos[\Omega_*|t-T| - \phi] e^{-\beta_{tot}|t-T|} - \cos[\Omega_*(t+T-2L/c) - \phi] e^{-\beta_{tot}(t+T-2L/c)} \right] \right\}. \quad (31)$$

The main contribution to this expression comes from the term in the second line of Eq. (31). The presence of small factor β_{tot} in the denominator indicates the resonance nature of bubble oscillations. During the process of leakage, bubbles can be produced in different sizes, but the time-reversal signal will excite them at its own natural frequency as it is a carrier frequency of the reversal wave.

Figure 5 illustrates variation in time of the bubble volume. The calculations have been carried out for the following values of determining parameters: $\Omega_*/(2\pi) = 1200$ Hz, $Q = 15$, $T = 100$ ms, $a = 30$ m, $L = 100$ m.

Calculations for more complex forms of the time-reversed signal Eq. (28), which describes the field in the waveguide can also be performed analytically. However, because the result looks very cumbersome and is reduced only to the increase in the amplitude of oscillations, we do not present these results here.

The back-scattered pressure $p^{bs}(\mathbf{r}, t_1)$ in the far field is described by formula (1). The signal emitted by these pulsations will exceed the original one, if the following condition is fulfillment: $g(R_0/L)\ (R_t/h)\ \arctan(a/L)\ (\Omega_*/2\beta) > 1$. To control the area with size of 100 m, it is necessary to gain the time-reversal signal relative to the incoming one more than three orders of magnitude.

The bubble birthing wail can be heard with source level as high as 110 dB (peak to peak) references to 1 μPa at a distance of 1 m.[9] Propagation at a distance of 100 m reduces the level of this signal by 40 dB. Ambient noise spectra level induced by bubbles and spray of surface agitation indicates near the same values in the kHz frequency range.[51,52] Thus the agitated state of the water interface is the limiting factor for the application of the proposed method.

Until now, a single bubble has been analyzed, which is an evident limitation to the real situation. The signal emitted by a bubble at its birth, in addition to that part that propagate to the array, is scattered by a cloud of bubbles that were born earlier and are rising over the vent. This scattering results in enhanced illumination of the array elements. But scattering of the time-reversed signal on the gas flare formed over the source is a much more important circumstance. The spatial extent of this signal is large enough, so for adopted scales of parameters, the wavelength is $\lambda_* \approx 1$ m, and the longitudinal size of the pulse is near 10 m. As a result, the time reversal signal is scattered by dozens, if not hundreds of bubbles, and, accordingly, the backscatter signal will increase by orders of magnitude. Discussion of features of time reversal technique accounting for multiple scattering on bubble clouds, in particular, considering focusing and waveguide effects caused by gas flare[4,6,8] is beyond the scope of the present work and is the subject of the future study.

V. DISCUSSION

In the current study, there has been technique proposed that involved counting the bubbles; however, that is only effective in measuring relatively slow leaks. In a sequestration site, or in a methane seep, one can expect much more than that. Increasing gas fluxes cause bubble signatures to overlap, and the preceding method requests modification. At the heart of the inversion method proposed for this case[11] is the assumption that the ambient noise measured by the hydrophone array is generated by a superposition of emissions from single bubbles for which Eqs. (2) and (4) are appropriate models. It is also assumed that the acoustic emissions of the bubbles are all uncorrelated, then the power spectral density, $\tilde{S}(\omega)$, of the far-field acoustic signature of the bubble cloud, at range r can be analyzed. In such circumstances, the individual bubble spectral signatures, and the bubble size distribution can be inverted from the overall spectrum. However, the phase relationship between the received pulse and the emitted time-reversal signal is important in time-reversal technique. For this reason, finding an effective method of digitizing the received random signal remains an unsolved problem.

There has been analyzed only one example of the implementation of TRM that is the linear vertical array. A one dimensional mirror allows finding the distance to the source. It is sufficient, in principle, for finding the possible location of the leak when the array is located near the underwater communications and its surrounding environment with known geometry. Use of two arrays operating with a time shift allows a reliable and unambiguous determination of the leak location in the region with unknown topography.

The sound environment of the ocean is an important aspect of marine habitat. There is growing concern that sound introduced into the sea by human activities has detrimental effects on marine life. Sounds of snapping shrimps produce the dominant level of ambient noise in shallow waters. The frequency spectrum of a snap is broad ranging from tens of Hz to 200 kHz. The snapping sound can be heard with source levels as high as 190–210 dB (peak to peak) references to 1 μPa at a distance of 1 m.[53] The snapping sound can be caught by the array, time-reversed, and focused on the shrimps as possible source. Because the physical nature of snaps is the formation of cavitation bubbles, these sounds are in the same frequency range as the leak emission. The array will not be able to distinguish the nature of sounds and can lead to a false alarm. Moreover, because to detect a leakage at distances of hundreds of meters the emission level should be large, this may lead to an undesirable contamination by anthropogenic noise the current water area.

The successful oceanic implementation of the discussed technique depends on practical constraints that can apply depending on the problem under consideration. Commercial devices to detect underwater leaks are relatively few. Naxys

develops and supplies leak detection and condition monitoring sensors based on proprietary, passive acoustic hydrophone technology. Co. L. Mar built a passive sonar system the main characteristic of which is the ability to detect and identify the acoustic signal generated by a leak. The underwater unit may be used on a vessel-towed "fish" or an ROV installation and has been successively used in a number of projects. To illustrate the possible solutions, three example applications have been detailed: Continuously monitoring a carbon sequestration site, continuous monitoring of a gas pipeline, and studying a methane seepage site.[11] In this study, we analyzed the scheme that is suitable for solving the first item in the preceding list. The time-reversal detection of waves with different intrinsic speeds (in pipe walls, water, seabed, or piped gas) offers another route to locating the sound source. The issues are different for methane seeps because these emit continuously, and so an alarm based on time-reversal acoustics is not usually useful. The time-reversal technique has advantages for research purposes in this case, as it allows to define more precisely the spectrum of bubble sizes produced at the seep. This occurs because the time-reversal signal has exactly the same carrier frequency as the one emitted by the birthing bubble.

VI. CONCLUSIONS

In this paper, a theory has been developed that allows one to increase the efficiency of subsea leak detection, which is important in the gas and petroleum industry. The proper description of the time reversal of the acoustic emission signals caused by the seepage from the seabed has been obtained. There are three major factors that provide effectiveness of the backscattering of the time-reversal wave from the bubble. The main effect is the refocusing of the bubble signature signal after time reversal at the original source location. The second factor is the presence of the bubble natural frequency in the reversed signal that leads to the resonant scattering. The third factor is the ability to re-emit the time-reversed signals with a significant gain. Analytical calculations are performed for the scattering of a time-reversal signal on a single bubble located near a rigid seabed.

ACKNOWLEDGMENTS

This study was supported by the RFBR, Project No. 14-05-00334a, and MES, Project No. SS-6084.2014.5.

[1]T. G. Leighton and A. J. Walton, "An experimental study of the sound emitted from gas bubbles in a liquid," Eur. J. Phys. **8**, 98–104 (1987).
[2]T. G. Leighton, *The Acoustic Bubble* (Academic, London, 1994), pp. 1–613.
[3]T. G. Leighton, P. R. White, and M. F. Schneider, "The detection and dimension of bubble entrainment and comminution," J. Acoust. Soc. Am. **103**, 1825–1835 (1998).
[4]R. Manasseh, A. Nikolovska, A. Ooi, and S. Yoshida, "Anisotropy in the sound filed generated by a bubble chain," J. Sound Vib. **278**, 807–823 (2004).
[5]E. M. B. Payne, S. J. Illesinghe, A. Ooi, and R. Manasseh, "Symmetric mode resonance of bubbles attached to a rigid boundary," J. Acoust. Soc. Am. **118**, 2841–2849 (2005).
[6]A. O. Maksimov, "Noise spectrum of a gas plume," Acoust. Phys. **51**, 435–442 (2005).
[7]I. Leifer and D. Tang, "The acoustic signature of marine seep bubbles," J. Acoust. Soc. Am. **121**, EL35–EL40 (2007).
[8]A. Nikolovska, R. Manasseh, and A. Ooi, "On the propagation of acoustic energy in the vicinity of a bubble chain," J. Sound Vib. **306**, 507–523 (2007).
[9]R. Manasseh, G. Riboux, and F. Risso, "Sound generation on bubble coalescence following detachment," Int. J. Multiphase Flow **34**, 938–949 (2008).
[10]C. A. Green and P. S. Wilson, "Laboratory investigation of a passive acoustic method for measurement of underwater gas seep ebullition," J. Acoust. Soc. Am. **131**, EL61–EL66 (2012).
[11]T. G. Leighton and P. R. White, "Quantification of undersea gas leaks from carbon capture and storage facilities, from pipelines and from methane seeps, by their acoustic emissions," Proc. R. Soc. London. Ser. A **468**, 485–510 (2012).
[12]J. Blackford, H. Stahl, J. M. Bull, B. J. P. Bergès, M. Cevatoglu, A. Lichtschlag, D. Connely, R. H. James, J. Kita, D. Long, M. Naylor, K. Shitashima, D. Smith, P. Taylor, I. Wright, M. Akhurst, B. Chen, T. M. Gernon, C. Hauton, M. Hayashi, H. Kaieda, T. G. Leighton, T. Sato, M. D. J. Sayer, M. Suzumura, K. Tait, M. E. Vardy, P. R. White, and S. Widdicombe, "Detection and impacts of leakage from sub-seafloor deep geological carbon dioxide storage," Nat. Climate Change **4**, 1011–1016 (2014).
[13]M. Fink, "Time reversal of ultrasonic field. Part I: Basic principles," IEEE Trans. Ultrason. Ferroelectr. Freq. Control **39**, 555–566 (1992).
[14]M. Fink, "Time reversed acoustics," Phys. Today **50**(3), 34–40 (1997).
[15]M. Fink, D. Cassereau, A. Derode, C. Prada, P. Roux, M. Tanter, J. L. Thomas, and F. Wu, "Time reversed acoustics," Rep. Prog. Phys. **63**, 1933–1995 (2000).
[16]M. Fink and C. Prada, "Acoustic time-reversal mirrors," Inverse Problems **17**, R1–R38 (2001).
[17]D. R. Jackson and D. R. Dowling, "Phase conjugation in underwater acoustics," J. Acoust. Soc. Am. **89**, 171–181 (1991).
[18]W. A. Kuperman, W. S. Hodgkiss, H. C. Song, T. Akai, T. Ferla, and D. Jackson, "Phase conjugation in the ocean: Experimental demonstration of an acoustic time-reversal mirror," J. Acoust. Soc. Am. **103**, 25–40 (1998).
[19]W. Hodgkiss, H. Song, W. Kuperman, T. Akai, T. Ferla, and D. Jackson, "A long range and variable focus phase-conjugation experiment in shallow water," J. Acoust. Soc. Am. **105**, 1597–1604 (1999).
[20]H. C. Song, W. A. Kuperman, W. S. Hodgkiss, T. Akal, and C. Ferla, "Iterative time reversal in the ocean," J. Acoust. Soc. Am. **105**, 3176–3184 (1999).
[21]J. S. Kim, H. C. Song, and W. A. Kuperman, "Adaptive time-reversal mirror," J. Acoust. Soc. Am. **109**, 1817–1825 (2001).
[22]S. Kim, W. A. Kuperman, W. S. Hodgkiss, H. Song, G. F. Edelmann, and T. Akai, "Robust time reversal focusing in the ocean," J. Acoust. Soc. Am. **114**, 145–157 (2003).
[23]G. F. Edelmann, H. C. Song, S. Kim, W. S. Hodgkiss, W. A. Kuperman, and T. Akai, "Underwater acoustic communications using time reversal," IEEE J. Ocean. Eng. **30**, 852–864 (2005).
[24]P. Roux and W. A. Kuperman, "Time reversal of ocean noise," J. Acoust. Soc. Am. **117**, 131–136 (2005).
[25]H. C. Song, W. S. Hodgkiss, and W. A. Kuperman, "Improvement of time-reversal communications using adaptive channel equalizers," IEEE J. Ocean. Eng. **31**, 487–496 (2006).
[26]H. C. Song, W. S. Hodgkiss, W. A. Kuperman, W. J. Higley, K. Raghukmar, and T. Akal, "Spatial diversity in passive time reversal communications," J. Acoust. Soc. Am. **120**, 2067–2076 (2006).
[27]P. Roux, B. Roman, and M. Fink, "Time-reversal in an ultrasonic waveguide," Appl. Phys. Lett. **70**, 1811–1813 (1997).
[28]P. Roux and M. Fink, "Time reversal in a waveguide: Study of the temporal and spatial focusing," J. Acoust. Soc. Am. **107**, 2418–2429 (2000).
[29]P. Blomgren, G. Papanicolaou, and H. Zhao, "Super-resolution in time-reversal acoustics," J. Acoust. Soc. Am. **111**, 230–248 (2002).
[30]O. Couture, J.-F. Aubry, M. Tanter, and M. Fink, "Time-reversal focusing of therapeutic ultrasound on targeted microbubbles," Appl. Phys. Lett. **94**, 173901 (2009).
[31]M. Pernot, G. Montaldo, M. Tanter, and M. Fink, "Ultrasonic stars for time-reversal focusing using induced cavitation bubbles," Appl. Phys. Lett. **88**, 034102 (2006).
[32]J. Gatcau, L. Marsac, M. Pernot, J.-F. Aubry, M. Tanter, and M. Fink, "Transcranial ultrasonic therapy based on time reversal of acoustically induced cavitation bubble signature," IEEE Trans. Biomed. Eng. **57**, 134–144 (2010).
[33]M. Fink, A. Tourin, and J. De Rosny, "Auto-focalisation, communication and sonoluminescence with acoustic time reversal," in *Wave Scattering in*

Complex Media: From Theory to Applications. NATO Science Series. II. Mathematics, Physics and Chemistry, edited by B. van Tiggelen and S. Skipetrov (Springer, Dordrecht, Netherlands, 2003), Vol. 107, pp. 256–280.
[34]D. H. Chambers and A. K. Gautesen, "Time reversal for a single spherical scatterer," J. Acoust. Soc. Am. **109**, 2616–2624 (2001).
[35]Z. J. Waters, B. R. Dzikowicz, and H. J. Simpson, "Isolating scattering resonances of an air-filled spherical shell using iterative, single-channel time reversal," J. Acoust. Soc. Am. **131**, 318–326 (2012).
[36]D. V. Vlasov, E. A. Zabolotskaya, and Y. A. Kravtsov, "Acoustic phase conjugation in water containing bubbles," Sov. Phys. Acoust. USSP **29**, 69–70 (1983).
[37]E. A. Zabolotskaya, "Phase conjugation of sound beams in connection with 4-phonon interaction in a liquid containing gas-bubbles," Sov. Phys. Acoust. USSR **30**, 462–463 (1984).
[38]L. M. Kustov, V. E. Nazarov, and A. M. Sutin, "Phase conjugation of an acoustic wave at a bubble layer," Sov. Phys. Acoust. USSR **31**, 517–518 (1985).
[39]A. O. Maksimov, "Efficiency of acoustic phase conjugation in a liquid containing gas-bubbles," Sov. Phys. Acoust. USSR **35**, 53–56 (1989).
[40]V. Leroy, A. Bretagne, M. Fink, H. Willaime, P. Tabeling, and A. Tourin, "Design and characterization of bubble phononic crystals," Appl. Phys. Lett. **95**, 171904 (2009).
[41]A. Bretagne, A. Tourin, and V. Leroy, "Enhanced and reduced transmission of acoustic waves with bubble meta-screens," Appl. Phys. Lett. **99**, 221906 (2011).
[42]I. Leifer and R. K. Patro, "The bubble mechanism for methane transport from the shallow sea bed to the surface: A review and sensitivity study," Cont. Shelf Res. **22**, 2409–2428 (2002).
[43]T. G. Leighton, K. J. Fagan, and J. E. Field, "Acoustic and photographic studies of injected bubbles," Eur. J. Phys. **12**, 77–85 (1991).
[44]A. Vazquez, R. Manasseh, R. M. Sanchez, and G. Metcalfe, "Experimental comparison between acoustic and pressure signals from a bubbling flow," Chem. Eng. Sci. **63**, 5860–5869 (2008).
[45]A. O. Maksimov, B. A. Burov, A. S. Salomatin, and D. V. Chernykh, "Sounds of marine seeps: A study of bubble activity near a rigid boundary," J. Acoust. Soc. Am. **136**, 1065–1076 (2014).
[46]G. B. Deane and H. Czerski, "A mechanism stimulating sound production from air bubbles released from a nozzle," J. Acoust. Soc. Am. **123**, EL126–EL132 (2008).
[47]L. Borcea, G. Papanicolaou, and C. Tsogka, "Theory and applications of time reversal and interferometric imaging," Inverse Problems **19**, S139–S164 (2003).
[48]L. M. Brekhovskikh and Ju. P. Lysanov, *Fundamentals of Ocean Acoustics*, 3rd ed. (Springer, Berlin, 2003), Chap. 5. pp. 98–105.
[49]A. O. Maksimov, "On the volume oscillations of a tethered bubble," J. Sound Vib. **283**, 915–926 (2005).
[50]A. O. Maksimov and Yu. A. Polovinka, "Volume oscillations of a constrained bubble," Phys. Fluids **25**, 062104 (2013).
[51]G. M. Wenz, "Acoustic ambient noise in the ocean: Spectra and sources," J. Acoust. Soc. Am. **34**, 1936–1956 (1962).
[52]W. A. Kuperman and P. Roux, "Ambient noise," in *Springer Handbook of Acoustics*, edited by T. D. Rossing (Springer, New York, 2007), Pt. A, Chap. 5., Sec. 5.2.5, pp. 161–162.
[53]M. Versluis, B. Schmitz, A. von der Heydt, and D. Lohse, "How snapping shrimp snap: Through cavitation bubbles," Science **289**, 2114–2117 (2000).